The 9th European Congress on Computational Methods in Applied Sciences and Engineering
ECCOMAS Congress 2024
3 – 7 June 2024, Lisboa, Portugal

A NOVEL EHD-JET SYSTEM TO ACHIEVE A HIGH PERFORMANCE IN TERMS OF ENERGY CONSUMPTION AND HEAT TRANSFER

F. Dolati[1], M. khodkameh[2], J.C. Páscoa[3], M. Abdollahzadeh[3*]
[1] Faculty of Mechanical Engineering, University of Guilan, Rasht, Iran,
farid.dolati@gmail.com
[2] Faculty of Mechanical Engineering, University of Guilan, Rasht, Iran,
mahsankhodkameh1378@gmail.com
[3] Department of Electromechanical Engineering, C-MAST- Center for Mechanical and Aerospace Science and Technology, Universidade da Beira Interior, Covilha - 6201 001, Portugal.,
mm.abdollahzadeh@ubi.pt, pascoa@ubi.pt

Key words: Electrohydrodynamic Jets; Numerical Simulation; Heat Transfer Enhancement;

ABSTARCT

Electrohydrodynamic (EHD) is the study of the interactions between an electric field and fluid flow field. This is obvious that an electric field can impress on the behavior of a fluid flow. In the event that ionization of air is present it leads to an induced flow as corona wind or ionic wind. Corona wind is created by electric discharge at a high voltage (in the kV range). While the applied voltage may be high, the current intensity is usually small (in the range varying from μA to mA). This indicates that power consumption has an amount almost negligible that this energy-efficient feature of corona wind can be used in many industrial processes such as cooling. A numerical investigation has been conducted to study the effect of shape of ground collector on gas velocity and electric energy consumption for a wire-plate type EHD-jet. It was numerically revealed that the flow features as well as performance of electrohydrodynamically induced gas flow in a wire-plate electrode system were changed depending on the shape of the grounded electrode. Moreover, numerical results showed the gas velocity for the cases of curve grounded electrode to that for the case of flat grounded electrodes have positive sides in aspect of cooling and energy consumption. Besides, the gas velocity increases with increasing applied voltage.

1 INTRODUCTION

With demanding of minimizing energy consumption accompanied by miniaturizing devices, researchers have been compelled to spend a great deal of effort to attain higher performances. Electrohydrodynamics (EHD), as an active method, enables industries to go beyond the limits. It is one of the more promising methods among various techniques because of its several advantages, e.g. low energy consumption, short response time, compatibility with chips and chip-level structures and controllable air flow without moving parts. The mechanism of this approach involves the interactions between electric field, flow field, and temperature field. Under a high voltage applied to a corona electrode, the air in its vicinity ionized and reveals as the corona discharge. A great aspect of corona discharge is the generation of corona wind. This phenomenon is caused by the migration of the ions, propelled by the Coulomb force, from the corona electrode toward the collector electrode. During the travelling, the ions impart their

momentum to neutral molecules via collision. This leads to formation of a bulk flow known as corona wind. The characteristics of corona discharge are dependent mainly on the device configuration, which are mostly specified by the purpose of its application and directly affect the energy efficiency. Applying a high voltage has applications in various fields and is considered a highly powerful tool for improving combustion processes [1,2], drying wet materials [3], controlling fluid flow [4], enhancing natural convection heat transfer [5], and increasing forced convection heat transfer [6].

Takeuchi et al. [7] examined the effects of discharge electrode parameters on the flow velocity distribution of a wire-rod type electrohydrodynamic gas pump. Upon applying high voltage to the wire, they observed a gas flow generated in the direction from the wire electrode toward the rod electrode in atmospheric air.

A new design of collecting electrodes, comprising different grounded electrode arrangements in two types of wire and plate, was examined by Taghavi Fadaki et al. [8]. Their numerical evaluations confirmed that, in terms of thermal enhancement factor, the electrohydrodynamic phenomenon with collecting wires can be more effective in comparison to the case with the grounded plate. Nonetheless, it is more cost-effective to employ plate collector than wire collector, since it has higher EHD efficiency. They also observed a negative effect on the heat transfer enhancement in some specific conditions which depends upon the Reynolds number and applied voltage values.

Regarding the above mentioned reports, the device configuration significantly affects the corona discharge performance. As well, the type of collecting electrode is directly related to the corona wind direction. Nevertheless, few researchers have studied the effect of grounded electrode on the flow characteristics and electric power consumption, which is the main purpose of this paper.

2. MATHEMATICAL METHODOLOGY

2.1. Physical model

A structure similar to the one proposed by Tsubone et al. [9], which will also be used for validation in later sections, has been selected as the reference model for this study due to its compactness and simplicity. The schematic of the physical model with dimension is shown in Figure 1.

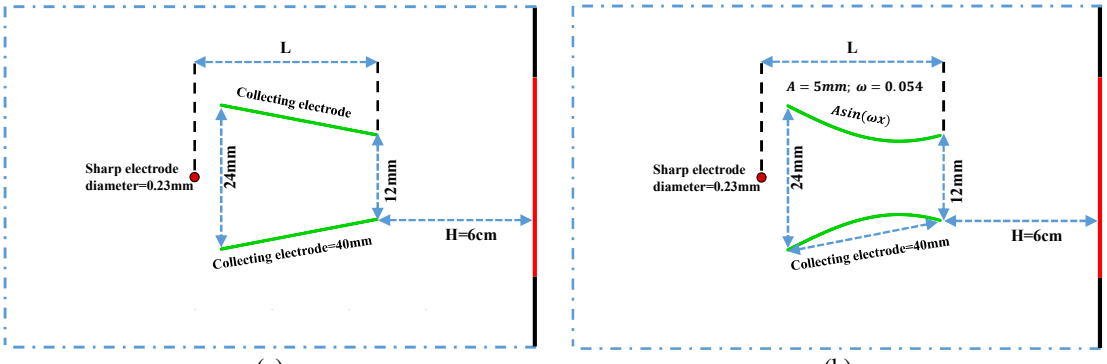

Figure 1. Schematics of the reference case used in the present study: (a) Flat collector (conventional type); (b) Curved collector (novel design).

2.2. Electro-hydrodynamic governing equations

The equations governing the electro-hydrodynamic part of the problem include Gauss's law and electric charge continuity equations which are given as follows [8]:

Gauss's law:

$$\nabla.(\epsilon\vec{E}) = \rho_c \tag{1}$$

Electric charge continuity:

$$\frac{\partial\rho_c}{\partial t} + \nabla.\vec{J} = 0 \tag{2}$$

where ρ_c, $\vec{E}$, ϵ are charge density, electric field and fluid permittivity, respectively. Also, $\vec{J}$ the current density vector and $\vec{E}$ the electric field vector in equations (1) and (2) are defined as:

$$\vec{E} = -\nabla\varphi \tag{3}$$

$$\vec{J} = \rho_c\overrightarrow{u_d} + \rho_c\vec{u} - D\nabla\rho_c \tag{4}$$

In equation (4) $\vec{u}$ is the flow velocity and $\overrightarrow{u_d}$ is the drift velocity which causes the collision of the ions of fluid and neutral molecules and it is described by:

$$\overrightarrow{u_d} = b\vec{E} \tag{5}$$

In equation (5) b is the ion mobility. The terms $\rho_c\vec{u}$ and $D\nabla\rho_c$ have infinitesimal amounts compared to the first term of the equation (4) and are negligible [10]. Thus, the equation (4) would turn into the following equation:

$$\vec{J} = \rho_c b\vec{E} \tag{6}$$

Using Equations (6) and (3), the main governing equations (equations (1) and (2)) are simplified as:

$$-\nabla^2\varphi = \frac{\rho_c}{\epsilon} \tag{7}$$

$$\frac{\partial\rho_c}{\partial t} - \nabla.(b\rho_c\nabla\varphi) = 0 \tag{8}$$

The net effect of the presence of high electric field and a region of ionized particles is an electrohydrodynamic body force $\overrightarrow{F_e}$ which must be taken into account in the governing equation of the fluid, see equation (15).

2.3. Governing equations of fluid flow and energy transfer

The working fluid is air at room temperature, and it is considered to be single phase, incompressible, and the presence of gravitational forces is neglected. The equations governing the fluid flow and energy transfer in steady state are as follows [11]:

Continuity equation:

$$\frac{\partial(\rho u_i)}{\partial x_i} = 0 \tag{9}$$

Momentum equation:

$$\frac{\partial}{\partial x_i}(\rho u_i u_j) = -\frac{\partial p}{\partial x_i} + \frac{\partial}{\partial x_j}\left[(\mu+\mu_t)\left(\frac{\partial u_i}{\partial x_j} + \frac{\partial u_j}{\partial x_i}\right)\right] + F_{e_i} \tag{10}$$

The eddy viscosity is computed from:

$$\mu_t = \rho C_\mu \frac{k^2}{\varepsilon} \tag{11}$$

The Realizable *k-ε* turbulence model has been chosen to treat the turbulence flow and heat transfer. This model had shown to be compatible to EHD problems. This turbulence model has been shown to be particularly effective in predicting turbulence characteristics in impinging jet

flows, which are relevant to the flow control system studied here. The governing equations of the Realizable k-ε turbulent model are as follows:

$$\frac{\partial(\rho k u_j)}{\partial x_j} = \frac{\partial}{\partial x_j}\left(\left(\mu + \frac{\mu_t}{\sigma_k}\right)\frac{\partial k}{\partial x_j}\right) + G_k - \rho\varepsilon \tag{12}$$

$$\frac{\partial(\rho \varepsilon u_j)}{\partial x_j} = \frac{\partial}{\partial x_j}\left(\left(\mu + \frac{\mu_t}{\sigma_\varepsilon}\right)\frac{\partial \varepsilon}{\partial x_j}\right) + C_1\rho S\varepsilon - C_2\rho\frac{\varepsilon^2}{k+\sqrt{\vartheta\varepsilon}} \tag{13}$$

In the above equations, G_k is the production of the turbulent kinetic energy due to mean flow velocity. Also, the constant C_1 is also defined as:

$$C_1 = max\left\{0.43, \frac{\eta}{\eta+5}\right\}, \eta = S\frac{k}{\varepsilon}, S = \sqrt{2S_{ij}S_{ij}} \tag{14}$$

where S_{ij} is the strain rate.

The last term in the right hand side of equation (10) is the electrohydrodynamic body force and is defined as follows:

$$\overrightarrow{F_e} = \rho_c\vec{E} - \frac{1}{2}|E|^2\nabla\epsilon + \frac{1}{2}\vec{\nabla}\left[|E|^2\rho\frac{\partial\epsilon}{\partial\rho}\right] \tag{15}$$

The term $\rho_c\vec{E}$ in equation (15) is known as the Coulomb force and possesses a remarkable share of the magnitude of the induced source term. For corona discharge in air under atmospheric pressure and at room temperature, electric permittivity can be assumed to be constant for a single phase fluid. Therefore, the terms $\frac{1}{2}|E|^2\nabla\epsilon$ and $\frac{1}{2}\vec{\nabla}\left[|E|^2\rho\frac{\partial\epsilon}{\partial\rho}\right]$ can be ignored [6]. Thus, the EHD induced body force in the momentum equation can be expressed as:

$$\overrightarrow{F_e} = \rho_c\vec{E} \tag{16}$$

Energy equation:

$$\frac{\partial}{\partial x_i}\left[\rho c_p u_i T\right] = \frac{\partial}{\partial x_j}\left[\left(K + \frac{c_p\mu_t}{\mathrm{Pr}_t}\right)\frac{\partial T}{\partial x_j}\right] \tag{17}$$

Where C_p is the specific heat coefficient, K is the thermal conductivity of the flow, T is flow temperature, and Pr_t is the turbulent Prandtl number.

2.4. Boundary conditions of the mathematical model

The value of the electric potential at different boundaries, including the electrodes, is known and determined. However, it is not easy to determine the value of the boundary condition of electric charge density on the electrode. Several methods have been proposed to calculate the amount of charge density on the emitting electrode. However, due to the lack of experimental data on the electric current, the Kaptzov hypothesis is used to determine the charge density on the emitting electrode. The Kaptzov hypothesis provides a path that can be directly used in numerical analysis to find the amount of charge density. In this method, an initial estimate of the charge density on the injecting electrode is made. The magnitude of the electric field at the injecting electrode is then calculated through numerical analysis. If there is a discrepancy between the electric field magnitude obtained from Peek's formula and the numerical analysis, the charge density on the injecting electrode is adjusted, and a new estimate is selected. This process is repeated until the magnitude of the electric field obtained from the numerical analysis closely matches the value derived from Peek's formula. Peek presented a relationship for the maximum value of the electric field on a cylindrical electrode after the commencement of the corona current as follows [12]:

$$E_{Peek} = 3.1 \times 10^6 \left(1 + \frac{0.308}{\sqrt{r_w}}\right) \quad (21)$$

In this equation, r_w is the radius of the electrode in centimeters. The boundary conditions applied to the present numerical model are shown in Figure 2.

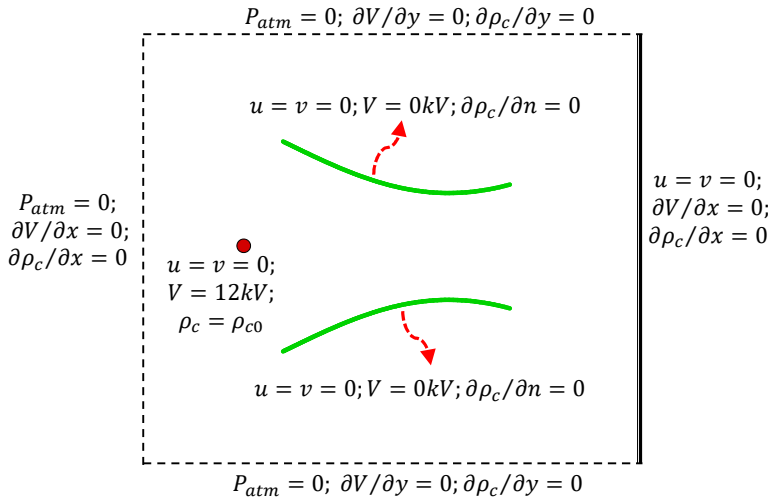

FIGURE 2. Flow filed and electric fields boundary conditions.

3. NUMERICAL PROCEDURE AND GRID INDEPENDENCY TEST

Given the assumptions made, only the governing equations for the fluid flow field are dependent on the electric field. Therefore, to perform the numerical estimation of the governing equations, the equations governing the electric field must be solved first (Equations (7) and (8)), followed by the flow and energy equations.

In this study, the geometry and computational grid were generated using Pointwise software version 18.3. The grid is structured, non-uniform, and rectangular, with higher density in regions where steep gradients are expected. For instance, the electric field parameters around the emitting and collecting electrodes and the velocity variations near the walls exhibit significant gradients. Therefore, as shown in Figure 2, the grid density in these areas is higher than in other regions. Additionally, the computational domain has been divided into several sections to allow for better control over the generated grid. For example, around the electrodes, different blocks have been considered to create a structured grid and ensure appropriate grid density. To achieve grid-independent results, the average velocity at the exit of nozzle was examined for various grids. Finally, the average velocity for grids with 64,680 and 89,140 cells is nearly identical. Therefore, to reduce computational costs in the numerical analysis, the grid with 64,680 cells was selected.

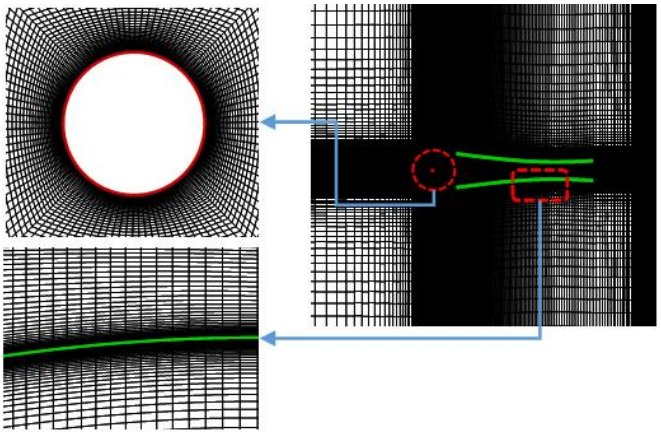

FIGURE 3: A schematic of the computational mesh used for the simulation.

4. VALIDATION

For the validation, the results of the numerical simulation were compared with the experimental results of Tsubone *et al.* [9]. The wire was placed midway through the channel length and the grounded electrodes are inclined at the angle of 3 degrees. The working fluid is air and its properties are assumed to be constant. The air properties at room temperature and atmospheric pressure are indicated in Table 1.

Table 1. Air properties used in the numerical simulation.

Property	Value	Unit
Density, ρ	1.225	$\mathrm{kg/m^3}$
Viscosity μ	$1.78e \times 10^{-5}$	$\mathrm{kg/m.s}$
Heat capacity, c_p	1006.43	$\mathrm{J/kg.K}$
Thermal conductivity, k	0.0242	$\mathrm{W/m.K}$

The results of the numerical simulation results of different turbulence models and the laminar model for the discharge current and average flow velocity at 5 mm downstream of the outlet of the channel, as a function of the applied voltage, are compared with the experimental results of Tsubone *et al.* [9] in Fig. 4. It can be seen that the numerical results are well in line with the experimental data; the disparity between the experimental data and the current simulations is less than 5%. Therefore, the reliability of the numerical model can be assumed verified.

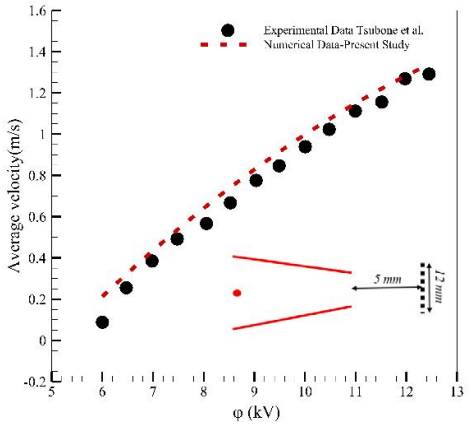

FIGURE 4. Validation of the numerical results in comparison with the experimental data of [9] for average velocity at a vertical line 5 mm downstream of the outlet of the channel.

5. RESULTS AND DISCUSSION

Figs. 5 illustrates the electric field vector, space charge density distribution and velocity vector. Fig. 5a shows electric field vectors which move outward from corona wire to the grounded plate and are concentrated at both electrodes. In addition, the space charge is centered around the emitting electrode and spreads downwards to the collecting electrode (Fig. 5b). Therefore, the maximum values of electric body force are generated in the region around the corona wire which clearly is obvious around the emitting electrode.

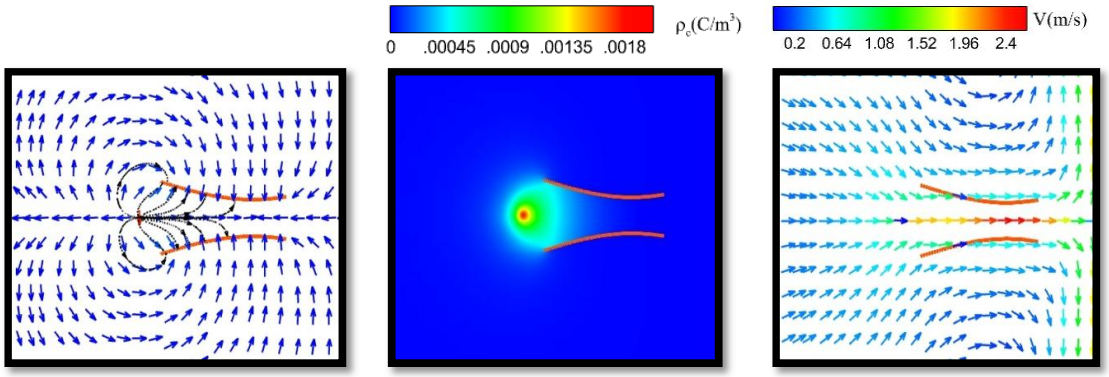

(a) (b) (c)

FIGURE 5. Distribution of (a) electric field vectors; (b) space charge density distribution.

Fig. 6 highlights the impact of increasing the applied voltage on the generation of body force and the formation of secondary flow due to ionization. As the voltage increases, more ionization occurs in the environment, leading to the production of more electric charges. These electric charges, create stronger bulk flow.

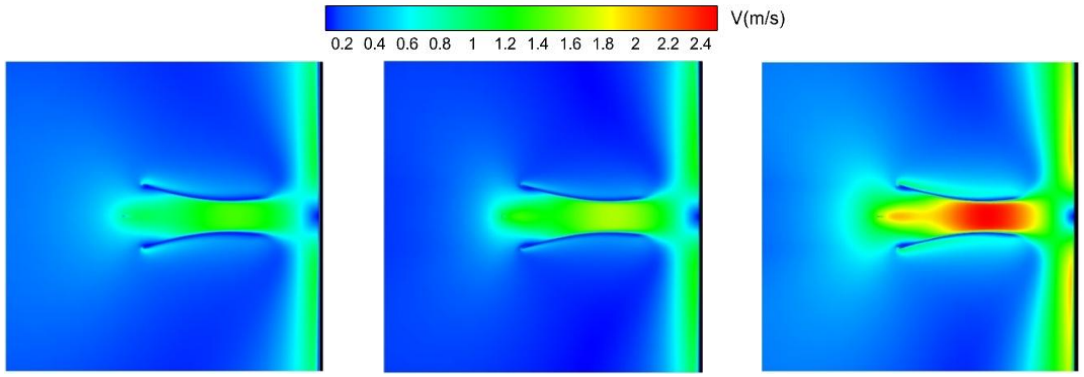

FIGURE 6. The effect of applied voltage: (a) 10kV; (b) 12kV; (c)14 kV.

In order to evaluate the effect of position of the emitting electrode (L) on both configurations (flat and curve) on flow pattern, three locations were considered. Fig. 6 depicts the velocity contours for the different configurations of electrode positions in the horizontal direction. It is clear that the horizontal position variation of electrode causes considerable changes in the flow pattern. It seems that there is an optimum point to produce maximum velocity. It is highlighted that the shape of grounded collector strongly affects Coulomb force as well as electric fields distribution which directly corresponds to flow pattern. In this regard, the effect of the shape of grounded collector (flat and curve) on the airflow is examined in Fig. 7. As would be observed, using a curve electrode results in the complexity of the flow pattern and makes massive and strong bulk flow in the nozzle.

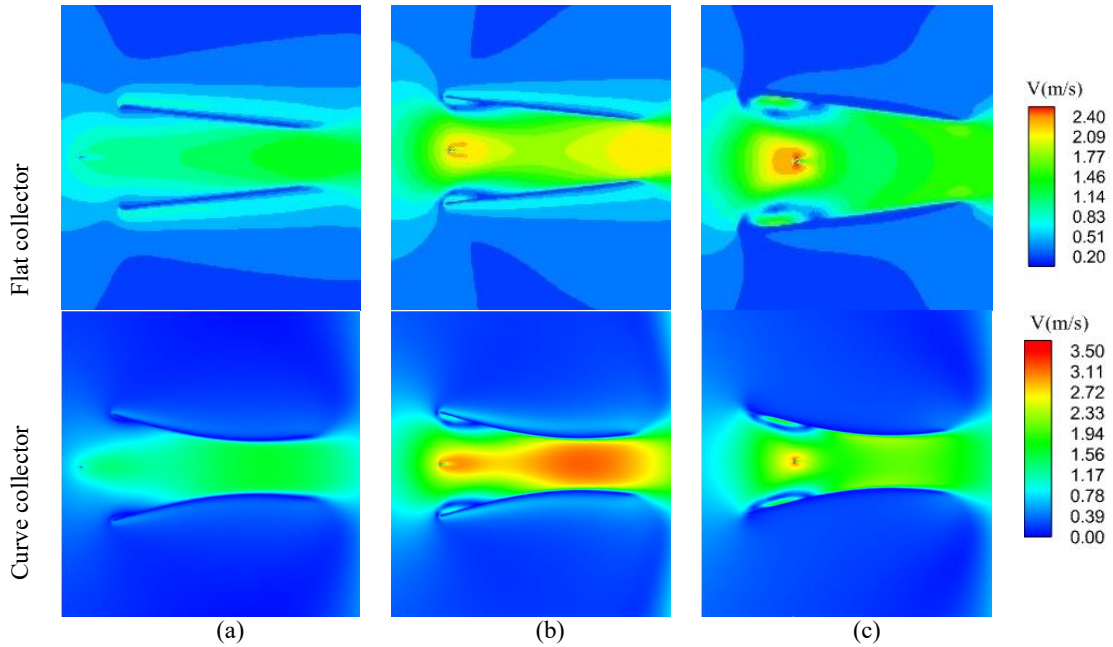

FIGURE 7. Flow field at different location of emitting electrodes: (a) L=4.7cm; (b) L=4cm; (c) L=3cm.

Achieving to a system with a high velocity does not guaranty to find an optimum and appropriate configuration. In fact, other parameters such as electric power consumption as well as the efficiency of system must be checked. Fig. 8 displays the effect of location of emitting electrode on average velocity, electric power consumption and efficiency. It can be seen that after a specific distance (L>4cm), the average velocity in the curved configuration is lower than in the flat configuration. As the distance increases, the electric energy consumption decreases in both scenarios. Additionally, at greater distances, the energy consumption for the curved configuration is much higher than for the flat configuration. Finally, in aspect of efficiency, although the curved configuration has a higher average velocity, it does not have more effective performance compared to the flat configuration. To understand why these conditions have occurred, the physics of the flow in the curved configuration needs to be examined more closely, and a solution should be proposed to address it. By understanding the flow physics, our suggestion is to use a novel collector, part of which is connected to the ground.

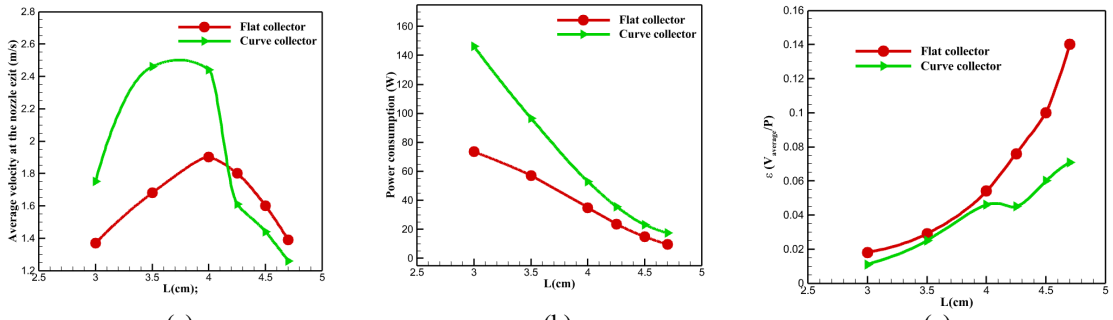

(a) (b) (c)

FIGURE 8. Effect of location of emitting electrode on: (a) average velocity; (b) power; (c) efficiency.

In Fig. 9, the streamlines for cases where part of the collector electrode is connected to the ground is shown. As can be seen, with the increase in the angle (a measure to specify the region connected to the ground), the "vena contracta", as a barrier, significantly decreases.

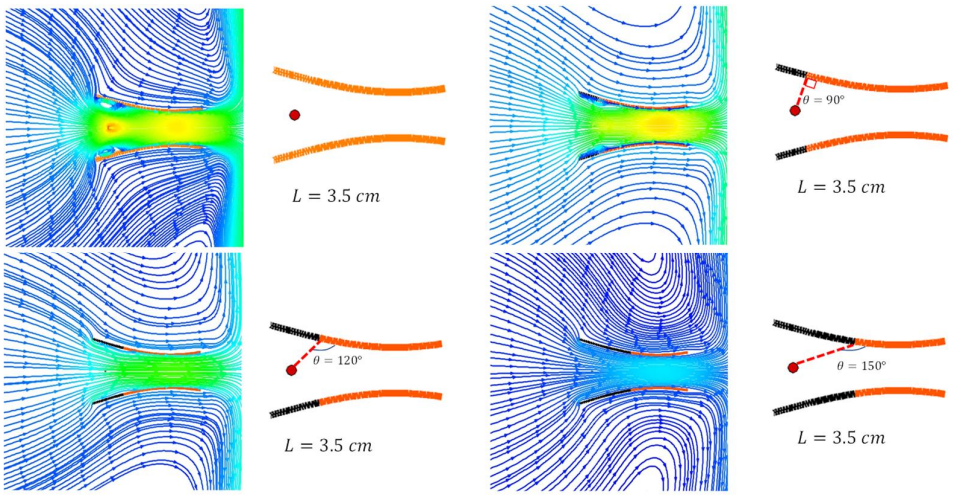

Figure 9. Streamlines at different configurations.

Fig. 10 depicts the effect of partially grounded electrode on average velocity ratio, electric power consumption ratio and efficiency ratio. With changing in the amount of the collector, it is observed that while maintaining the advantage in average velocity, the power consumption has also decreased (Fig10a). Therefore, according to Fig. 10b, the performance of system performance has improved compared to the flat configuration.

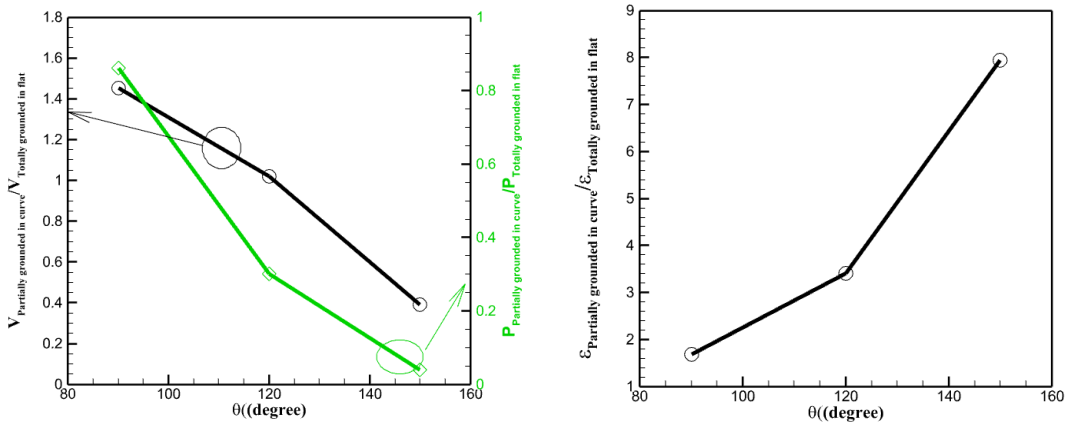

(a) (b)

FIGURE 10. The effect of partially grounded electrode on: (a) average velocity ratio, electric power consumption ratio; (b) efficiency ratio.

6. CONCLUSION

According to the numerical achievements, it can be clearly seen that the flow pattern and electric energy consumption strongly depend the grounded electrode. The main findings of the present work are as below:

- The voltage applied to the wire has a direct relationship with both the mean velocity at the nozzle exit and power consumption.
- In both types of collecting electrodes, increasing the value of L from its lower bound to the center point value causes the mean velocity to increase, while further increasing its value results in reduction of the mean velocity at the nozzle exit.
- By increasing the parameter L electric power consumption saw a significant decrease due to growth in distance between electrodes.
- In the first prototype of collecting electrode (curve collector), the performance of EHD-jet system, ε, did not show an improvement.
- By applying partially grounded electrode, the performance of EHD-jet system (ε) witnessed a considerable enhancement.

The proposed EHD system is highly power efficient, with a high performance gas blower, making it an ideal choice for cooling electronic devices or other objects in compact areas where the installation of fans or other cooling devices is not feasible. Additionally, our proposed EHD system has the advantage of being suitable for cooling applications in areas where rotary systems cannot be utilized.

ACKNOWLEDGMENTS

Authors acknowledge the support by Portuguese national funds by FCT-Foundation for Science and Technology, within the unit C-MAST - UIDB/00151/2020 (https://doi.org/10.54499/UIDB/00151/2020) and UIDP/00151/2020 (https://doi.org/10.54499/UIDP/00151/2020).

REFERENCES

[1] S. Khasare, F. Bagherighajari, F. Dolati, J. Mahmoudimehr, J.C. Pascoa, M. Abdollahzadeh, Control of the flame and flow characteristics of a non-premixed bluff body burner using dielectric barrier discharge plasma actuators, Appl. Therm. Eng. 235 (2023) 121432. doi:10.1016/J.APPLTHERMALENG.2023.121432.

[2] S. Khasare, F. Bagherighajari, F. Dolati, J. Mahmoudimehr, J. Páscoa, M. Abdollahzadehsangroudi, The effect of the dielectric barrier discharge plasma actuator in the control of non-reactive flow in a non-premixed bluff body burner, Phys. Fluids. 35 (2023) 075135. doi:10.1063/5.0157976/2902906.

[3] F. Dolati, N. Amanifard, H.M. Deylami, A combined technique for drying enhancement of porous bodies using multiple obstacles in presence of ehd actuator through a smooth channel, J. Porous Media. 24 (2021) 1–20. doi:10.1615/JPORMEDIA.2021033403.

[4] A. Kadivar, N. Amanifard, H.M. Deylami, F. Dolati, Flow separation control in an axial compressor cascade using various arrangement of plasma actuator, J. Electrostat. 112 (2021) 103580. doi:10.1016/J.ELSTAT.2021.103580.

[5] S.S.M. Golsefid, N. Amanifard, H.M. Deylami, F. Dolati, Numerical and experimental study on EHD heat transfer enhancement with Joule heating effect through a rectangular enclosure, Appl. Therm. Eng. 123 (2017) 689–698. doi:10.1016/J.APPLTHERMALENG.2017.05.129.

[6] H.M. Deylami, N. Amanifard, F. Dolati, R. Kouhikamali, K. Mostajiri, Numerical investigation of using various electrode arrangements for amplifying the EHD enhanced heat transfer in a smooth channel, J. Electrostat. 71 (2013) 656–665. doi:10.1016/j.elstat.2013.03.007.

[7] N. Takeuchi, K. Yasuoka, J.S. Chang, Effect of discharge electrode parameters on the flow velocity profile of the wire-rod type electrohydrodynamic gas pump exit, IEEE Trans. Dielectr. Electr. Insul. 16 (2009) 615–621. doi:10.1109/TDEI.2009.5128496.

[8] S.S. Taghavi Fadaki, N. Amanifard, H.M. Deylami, F. Dolati, Numerical analysis of the EHD driven flow with heat transfer in a smooth channel using multiple collectors, Heat Mass Transf. Und Stoffuebertragung. 53 (2017) 2445–2460. doi:10.1007/s00231-017-1994-7.

[9] H. Tsubone, J. Ueno, B. Komeili, S. Minami, G.D. Harvel, K. Urashima, et al., Flow characteristics of dc wire-non-parallel plate electrohydrodynamic gas pumps, J. Electrostat. 66 (2008) 115–121. doi:10.1016/j.elstat.2007.09.002.

[10] R. Baghaei Lakeh, M. Molki, Targeted heat transfer augmentation in circular tubes using a corona jet, J. Electrostat. 70 (2012) 31–42. doi:10.1016/j.elstat.2011.09.003.

[11] J. Wang, X. Hu, X. Mo, Z. Sun, R. Fu, Flow and heat transfer characteristics of corona wind in two symmetric divergent fins, Int. J. Heat Mass Transf. 160 (2020) 120210. doi:10.1016/J.IJHEATMASSTRANSFER.2020.120210.

[12] M.L. Amrani, S. Bouazabia, I. Fofana, F. Meghnefi, M. Jabbari, Modified Peek formula for calculating positive DC corona inception voltage on polluted insulator, Electr. Eng. 101 (2019) 489–498. doi:10.1007/s00202-019-00797-7.